Evaluation of numerical pounding models with experimental validation

S. Khatiwada, N. Chouw & J.W. Butterworth

The University of Auckland, Auckland, New Zealand.

2013 NZSEE Conference

ABSTRACT: Pounding damage in major earthquakes has been observed frequently in the form of aesthetic, minor or major structural cracks and collapse of buildings. The observations have attracted many numerical and experimental studies that led to analytical models for simulating seismic pounding. This study considers pounding between two steel portal frames without a seismic gap. The first frame has a constant natural period while the second frame has variable stiffness and mass values. Five different ground motions are applied to eight combinations of adjacent frames using a shake table. Numerical simulations for the same configurations are carried out with five pounding force models. The contact element stiffness and coefficient of restitution for numerical models are determined experimentally. The amplification of maximum displacement of the first frame predicted by the numerical simulations is compared with the shake table results, revealing that the linear viscoelastic contact element model gives the most accurate predictions

1 INTRODUCTION

Seismic pounding occurs when two adjacent structures or parts of a structure vibrate out of phase and the separation distance is too small to accommodate the relative displacement. The pounding causes the structures to exert repeated hammer like blows on each other which may cause minor non-structural or severe structural damage that may even lead to the complete collapse of buildings (Kasai and Maison 1997, Rosenbleuth and Meli 1985, Cole et al. 2011, Chouw and Hao 2012). Post-seismic surveys after almost all major earthquakes in urban areas have found the presence of damage due to pounding of buildings and bridges. Several urban seismic vulnerability surveys have identified pounding as one of the major hazards (Jeng and Tzeng 2000, Bothara et al. 2008). This has led to many numerical and experimental studies on pounding force (Jankowski 2005, Muthukumar and DesRoches 2006), building response (Papadrakakis and Mouzakis 1995, Chouw 2002), damage surveys and mitigation or prevention measures (Anagnostopoulos and Karamaneas 2008, Rezavandi and Moghadam 2007). These studies have resulted in the proposal of a number of analytical pounding force models for numerical simulations.

Seismic pounding is a form of impact where large impulsive forces act between the participating bodies resulting in a near-instantaneous change in momentum of the colliding bodies. The impact is called elastic if there is no loss of kinetic energy during the collision. If there is some energy loss, the impact is termed inelastic. Seismic pounding is a complex phenomenon involving heterogeneous materials, plane or fractal surface contact and effects of supporting structure and foundation system. There may be several collisions within a single earthquake and the impact velocities for each event will be different. As the current state of the art in pounding research cannot account for these factors, the numerical simulations include many assumptions such as lumped mass models, a constant coefficient of restitution and insensitivity of pounding forces to the contact surface geometry.

The lumped mass model assumes that the building frame or bridge deck acts as a diaphragm, and that the whole mass of the floor or deck contributes to the impact even though classical physics states that only a small part of the colliding mass participates in the contact (Goldsmith 2001). The model also assumes that the actual structural stiffness and the masses of the non-colliding floors above or below the pounding stories have no effect on the build-up of impulsive forces. During numerical simulations,

displacement of the structures are computed considering all structural properties but when the displacements time history of the neighbouring buildings intersect, the contact forces are calculated only from the colliding floor masses and relative velocity of impact.

The coefficient of restitution, defined as the ratio of the final relative velocity to the initial relative velocity of the colliding bodies, is employed as a measure of the elasticity of an impact. In an elastic impact, the coefficient of restitution equals one while it is zero for a completely plastic impact. Coefficient of restitution signifies the loss of kinetic energy due to several complex processes such as material damping, surface friction, surface yielding, residual internal vibrations, generation of sound and heat during collision etc. These processes are not fully understood even for the relatively simple collisions of identical spheres at known velocities. In the absence of large scale experimental results, the numerical simulations have to assume values based on the experiments on collision of small masses. The value is also assumed as invariable throughout the simulations even though past experiments have shown it varies according to the mass and the initial relative velocity of the colliding bodies (Goldsmith 2001).

Figure 1. Pounding damage observed in the 2011 Christchurch earthquake

The constraints and approximations have created a dichotomy in pounding research as most pounding models are proposed or derived based on measured pounding force and the numerical evaluation studies of these models also rely on structural acceleration, velocity and relative impact velocities while the researchers studying the effect of pounding on structures focus on amplification of structural displacement, bending moment, base shear and storey shear. Past studies have evaluated these models have either been based on single impact experiments which do not provide a measure of performance through a full ground motion. Shake table studies on pounding have usually evaluated only one model and performance have not been compared against other models.

To the authors' knowledge, no past study has attempted a parametric comparison of the predictions of various pounding models with experimental deformation amplification. This study presents the results of a shake table investigation of floor to floor pounding between two steel portal frames and compares them with the results from linear numerical analysis. A contact element model is recommended for use based on the comparison of predicted maximum displacement amplification with the experimental displacement amplification values. The contact elements are compared based on their displacement response because structural displacement has been found mostly insensitive to the contact element stiffness which cannot be determined with certainty. Structural drift is also the main kinematic parameter of interest to designers as all the internal forces in structures can be computed from displacement. The contact surface between the two frames was kept flat instead of the commonly employed hemispherical (Chau et al. 2003, van Mier et al. 1991) or cylindrical interfaces (Filiatrault, et al. 1995).

2 NUMERICAL MODELS FOR POUNDING FORCE

Numerical modelling has been employed frequently to predict pounding forces and structural responses. Such models define a constant "gap" between the buildings and if the relative closing displacement between the two buildings is more than the "gap", the contact force is activated. The most common form of contact model assumes the presence of an elastic spring with or without a viscous damper to model energy loss. These models have an advantage that they can be implemented in most existing numerical time history analysis software without significant programming modification. Other approaches like Lagrange and Laplace methods have also been employed in some studies (Chouw and Hao 2008, Papadrakakis et al. 1991) but their application is limited as they need special programming by the users or the modification to the current commercial software.

The aim of this study is to compare the results from various contact element models with the experimental results and select the best performing model. The linear elastic and nonlinear elastic contact elements cannot simulate inelastic impacts. Thus they have not been included in the comparison. The numerical models evaluated in the current study are described below with their underlying assumptions and their intended performance priorities, such as modelling energy loss or better prediction of pounding force.

2.1 **Linear viscoelastic model**

The linear viscoelastic model, also called the Kelvin model, has the same form as a Kelvin-Voigt material. It has a linear spring and a linear viscous damper in parallel. The pounding force is given by:

$$F = k.\delta(t) + c.\dot{\delta}(t); \qquad \delta(t) = (u_2(t) + \text{gap} - u_1(t)) \leq 0 \qquad (1)$$

$$= 0; \qquad \delta(t) = (u_2(t) + \text{gap} - u_1(t)) > 0$$

where gap is the original separation between the two structures, u_1 and u_2 are the displacements of the two masses, $\dot{\delta}(t)$ is their relative velocity, k is the impact element's stiffness, and c is the impact element's damping given by,

$$c = 2.\xi.\sqrt{k\frac{m_1 m_2}{m_1+m_2}} \qquad (1a)$$

where m_1 and m_2 are the colliding masses and ξ is the damping ratio given by

$$\xi = \frac{-\ln(e)}{\sqrt{\pi^2+\ln(e)^2}} \qquad (1b)$$

and e is the coefficient of restitution described earlier.

The formulations were first derived by Anagnostopoulos (1988). The expressions for the damping coefficient, c, and damping ratio, ξ, were derived so that the energy loss is the same as that in the stereo-mechanical model for the same e. The model, with respect to the displacement amplification of the structures, is found to be insensitive to the values of contact element stiffness. The impulsive acceleration calculated during impact varies according to the stiffness adopted, but this variation does not translate into variation in structural displacement. This model produces tensile force near the end of the contact which does not seem to agree with experimental force time histories. Several objections to the model's uniform damping throughout the contact have also been raised and several studies have proposed various amendments to the values of damping ratio which are discussed in latter sections.

2.2 **Modified linear viscoelastic model**

The modified element, also termed the 'Impact Kelvin element', has an approach only dashpot. Initially proposed by Valles and Reinhorn (1996), the impact Kelvin model has not been used in any numerical simulations, perhaps due to its complex formulation. The study also does not give any numerical investigation to show its performance.

A similar model, named the 'modified linear viscoelastic element', was later proposed by Mahmoud (2008), where the viscous damper is active only for the approach period, and the relationship between ξ and e in the linear viscoelastic element has been modified so that the total viscous damping can be incorporated within the approach period. The numerical formulations are given as:

$$F = k.\delta(t) + c.\dot{\delta}(t); \qquad \delta(t) = (u_2(t) + \text{gap} - u_1(t)) \leq 0, \dot{\delta}(t) > 0 \qquad (2)$$

$$= k.\delta(t); \qquad \delta(t) = (u_2(t) + \text{gap} - u_1(t)) \leq 0, \dot{\delta}(t) < 0$$

$$= 0; \qquad \delta(t) = (u_2(t) + \text{gap} - u_1(t)) > 0$$

where all the parameters are same as in the Kelvin-Voigt model, and c can be calculated using equation 1(b) but the damping ratio is given by:

$$\xi = \frac{1}{\pi}\frac{1-e^2}{e} \qquad (2b).$$

Mahmoud and Jankowski (2011) later proposed another formulation for the damping constant given as follows:

$$\xi = \frac{1-e^2}{e(e(\pi-2)+2)} \qquad (2c)$$

The two coefficients show only slight variation and the first formulation gives a value nearer to that of the linear viscoelastic model. Thus, equation (2b) is used for the numerical modelling in the current study.

The authors acknowledge that the modified formula is inferior to the original formulation in all their studied cases and recommend the original formula for use in the study of structural poundings (Mahmoud and Jankowski 2011). The modified model removed the tensile force from the F - δ relationship of the linear viscoelastic model but performed worse when compared with experimental results. Calculations show that, for the same stiffness and coefficient of restitution, the new formula not only removes the negative portion of the force but also gives higher positive results in the restitution portion of the F - t curve. This increases the total impulse and the effective coefficient of restitution is higher than the input value.

2.3 **Nonlinear viscoelastic model**

The nonlinear viscoelastic model was proposed by Jankowski (2005) to overcome the disadvantages of the linear viscoelastic, the nonlinear elastic models and to simulate structural pounding more precisely. This model adds a nonlinear viscous damper to the nonlinear elastic model. The viscous damper is active only when the masses approach each other, and thus the uniform damping and sticky force in the linear viscoelastic model are removed. The numerical formulations are:

$$F(t) = \bar{\beta}\,\delta^{3/2}(t) + \bar{c}\,\dot{\delta}(t); \qquad \delta(t) = (u_2(t) + \text{gap} - u_1(t)) \leq 0, \ \dot{\delta}(t) > 0 \qquad (3)$$

$$= \bar{\beta}\,\delta^{3/2}(t); \qquad \delta(t) = (u_2(t) + \text{gap} - u_1(t)) \leq 0, \ \dot{\delta}(t) \leq 0$$

$$= 0; \qquad \delta(t) = (u_2(t) + \text{gap} - u_1(t)) > 0$$

where $\bar{\beta}$ is the impact element stiffness and $\bar{c}(t)$ is the impact element's instantaneous damping which is defined as

$$\bar{c}(t) = 2\bar{\xi}\sqrt{\bar{\beta}\sqrt{\delta(t)}\frac{m_1 m_2}{m_1+m_2}} \qquad (3a)$$

where $\bar{\xi}$ is the damping ratio correlated with a coefficient of restitution e, (Jankowski 2006), e, as follows:

$$\bar{\xi} = \frac{9\sqrt{5}}{2} \cdot \frac{1-e^2}{e(e(9\pi-16)+16)} \quad (3b)$$

and other parameters are same as defined for the previous models.

Jankowski (2005) analysed and compared several experimental results against a linear viscoelastic model and a nonlinear viscoelastic model. The nonlinear viscoelastic model was found to be marginally better than the linear viscoelastic elastic model in predicting the pounding forces. The authors of the current study find it surprising that the linear elastic model performs nearly on a par with the nonlinear viscoelastic model. The former is optimized to model the energy lost in the system due to impact while the latter is optimized to match the pounding force time history.

The greatest strength of the nonlinear viscoelastic model is its ability to simulate the force time history better than the other existing models, if the stiffness and damping are known. However, it is handicapped by the inability to determine these parameters in advance. These parameters can be iteratively determined if the force time history is available but in the absence of such records its accuracy may not justify the extra complexity introduced in the calculations.

2.4 **Hertzdamp model**

The Hertzdamp model was introduced by Muthukumar and Desroches (2006) to enable the nonlinear elastic model proposed by Hertz to model inelastic pounding. The model had been used previously in robotics and mechanical engineering applications. The numerical formulation of the model is as follows:

$$F(t) = k\delta^{\frac{3}{2}}(t) + c\dot{\delta}(t); \qquad \delta(t) = (u_2(t) + \text{gap} - u_1(t)) \leq 0 \quad (4)$$

$$= 0; \qquad \delta(t) = (u_2(t) + \text{gap} - u_1(t)) > 0$$

where the nonlinear damping constant c is defined as

$$c(t) = \xi\delta^{\frac{3}{2}}(t) \quad (4a)$$

where the damping ratio ξ is given by,

$$\xi = \frac{3k(1-e^2)}{4\dot{\delta}_0} \quad (4b)$$

$\dot{\delta}_0$ is the relative velocity at the time of contact and all other parameters are the same as in previous models.

The Hertzdamp and nonlinear viscoelastic models both employ nonlinear viscous damping but while the nonlinear viscoelastic model assumes the damping during restitution is negligible, the Hertzdamp model assumes that, for a given value of relative penetration, δ, the damping constant is the same during deformation and restitution periods of contact.

2.5 **Modified Hertzdamp model**

Ye et al (2009) proposed a modification to Hertzdamp model because they found that the coefficient of restitution calculated from the output of the model was different from the initial value utilized in the computation. The error increased with decreasing value of the input coefficient. The edited formula for the damping ratio is given as,

$$\xi = \frac{8k(1-e)}{5e\dot{\delta}_0} \quad (5)$$

The force and damping relationships are the same as in the Hertzdamp model.

Ye et al. proved numerically that Equation 4(b) produces larger error for more inelastic contacts, and analytically derived expression (5) for damping ratio. The updated model removes a weakness of the

Hertzdamp model but introduces a possibility of negative tensile force near the end of contact.

3 **EXPERIMENTAL SETUP**

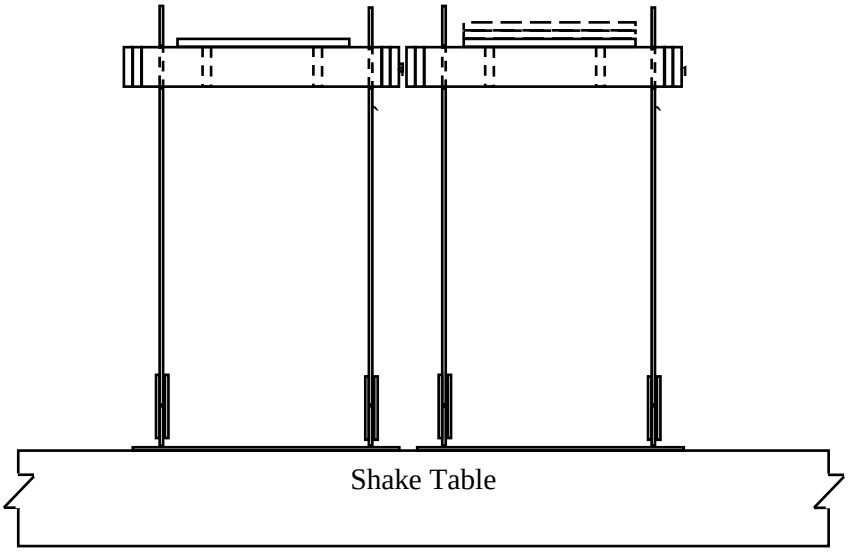

Figure 2. Schematic drawing of the experimental setup

The experiment was conducted on a displacement-controlled, 10 kN shake table located at the University of Auckland. It has a maximum displacement capacity of ±15 cm. Three different types of steel frames shown in Figure 2 were constructed. The three frames were all identical except for the column sizes which were 50 x 3 mm, 75 x 3 mm and 100 x 3 mm, respectively. The columns were 500 mm high, and supported two beams of section 50 x 10 mm. The beams supported a platform of dimensions 200 x 150 x 10 mm and were braced by two metal plates of size (column width) x 50 x 10 mm. The bases could also support an accelerometer each. The beams extended 2 cm outside either column, and were joined at each end by a 150 x 50 x 10 mm plate. On each end plate, another plate of the same size was screwed. These joined plates functioned as the actual pounding elements of the frames. During tests, the frames carried a flat plate on a side, and a plate with a 150 x 10 x 3 mm plate glued and welded to the flat plate on the other side. These plates ensured a flat surface contact during pounding. The stiffness values of the three frames are shown in Table 1. Extra masses of the same dimension could be attached to each platform. Since the plate dimensions are the same in all cases, the actual nodal mass of each type of frame is different. Table 2 assigns a mass ID for each mass configuration, and presents the value of mass for each mass ID for each frame type.

The medium stiffness frame (k2 = 8889 N/m) with the least mass (m0 = 8.04 kg) was selected as the reference frame. The medium stiffness facilitated the identification of the influence of increase and decrease in the other frame's stiffness. The least mass was selected for highest possible natural frequency because most previous studies have shown that the stiffer buildings in pounding suffer more displacement amplification. The mass and stiffness of the second frame was varied to produce different configurations. First, the stiffness of the second frame was kept same as the reference frame, and all four mass combinations were employed. Then, for constant mass (m0), the stiffness of the frame was varied. Finally, the tests were repeated with highest mass (m3) for both remaining stiffness because it has been observed that a building colliding with more massive building suffers more displacement amplification than when the second building's mass is similar. Table 3 shows the frame configurations that were employed for the test, their assigned frame IDs and the respective natural periods. Snap back tests were conducted to find the natural period and the damping constant of the structures. The actual periods of the frames were found to be within ±2% of the theoretical values. The damping ratio varied according to the tightness of the joints, the initial displacement of the structure and the mass on the frame, so an average damping ratio of 0.016 was adopted for the numerical analysis. Table 4 lists the frame pairings employed for the test and the resulting natural period ratio. Figure 3 shows the pounding arrangement for case 7.

Table 1. Stiffness ID for different frames

Column size (mm)	Stiffness ID	Stiffness (N/m)
50 x 3	k1	5926
75 x 3	k2	8889
100 x 3	k3	11,852

Table 2. Considered masses

Mass ID	Mass (kg)		
	k1	k2	k3
m0	8.04	8.59	9.14
m1	12.75	13.30	13.85
m2	17.46	18.01	18.56
m3	22.17	22.72	23.27

Table 3. Natural period T (s) for selected mass-frame combinations

Mass	Frame Stiffness		
	k1	k2	k3
m0	k1m0 T = 0.23	k2m0 T = 0.20	k3m0 T = 0.17
m1	-	k2m1 T = 0.24	-
m2	-	k2m2 T = 0.28	-
m3	k1m3 T = 0.38	k2m3 T = 0.32	k3m3 T = 0.28

Five selected time histories were applied to the models, viz. 1940 El-Centro ground motion, two artificial ground motions simulating the New Zealand design spectrum for hard soil condition and two from the Japanese design spectrum for hard soil condition. The simulated time histories were scaled down so that the absolute maximum ground deflection was ±10 cm. The El-Centro time history did not need to be scaled as its maximum deflection is only 8 cm. The scaled displacement time histories are shown in Figure 4. Henceforth, these time histories will be called El Centro, NZDS 1, NZDS 2, JDS 1 and JDS 2, respectively.

Each pairing of the frames was first placed on the shake table, far apart from each other and subjected to the five time histories to obtain their maximum displacement without pounding, u_{max}. Then each frame is placed adjacent to the reference frame, with zero separation gap, and subjected to the same time histories again. The zero separation was employed as past studies have found that the pounding response decreases as the gap size is increased. This is also a common configuration in old-style city blocks. The time histories were applied from both directions as the directional effect could have some effect on the pounding response. The displacement response of the frames was measured by the strain

gauges placed on the columns just below the beams. The strain gauges were calibrated against the displacement of each frame relative to its base. After the set of tests was finished, the calibration was checked again, and no difference was found between the initial and final calibrations. The pounding interface did not show any indentation or other permanent deformation after any of the tests.

Table 4. Period ratio of the frames considered

Case	Configurations (from Table 3)	T_2 (s)	T_1/T_2
1	k2m0-k1m0	0.23	0.84
2	k2m0-k1m3	0.38	0.51
3	k2m0-k2m0	0.20	1.00
4	k2m0-k2m1	0.24	0.80
5	k2m0-k2m2	0.28	0.69
6	k2m0-k2m3	0.32	0.61
7	k2m0-k3m0	0.17	1.12
8	k2m0-k3m3	0.28	0.70

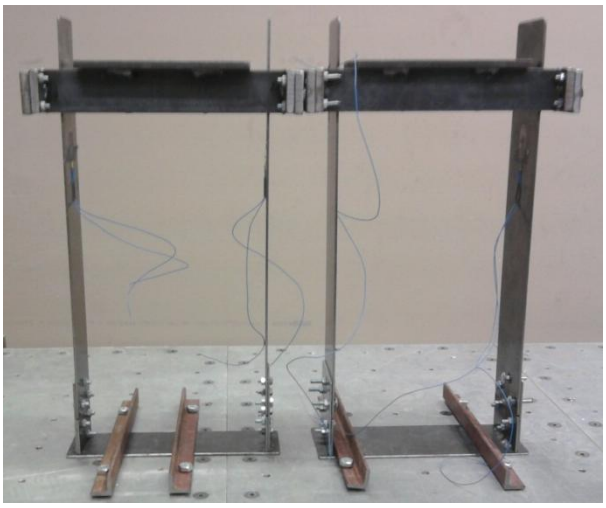

(a)

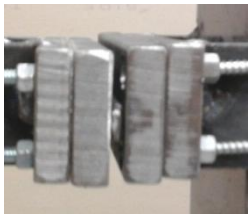

(b)

(c)

Figure 3. Adjacent structure without seismic gap: (a) Frames on shake table, (b) pounding interface and (c) Pounding elements

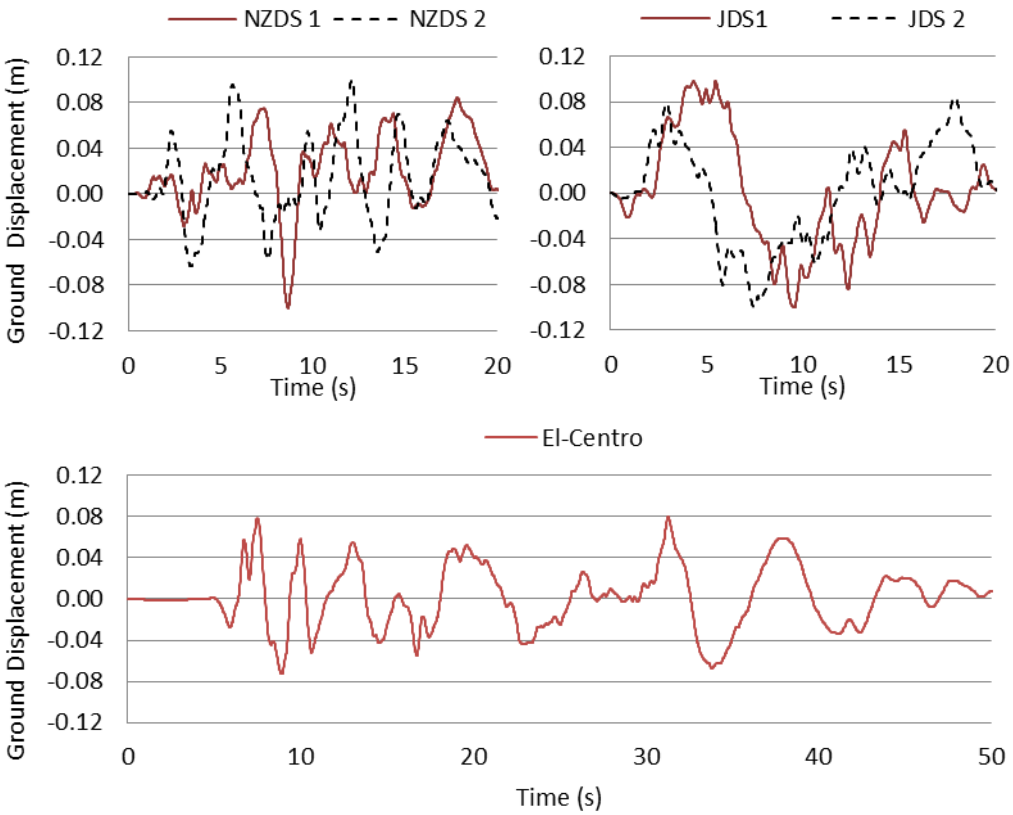

Figure 4. Ground motions considered

The impact element stiffness for the numerical force models and coefficient of restitution were determined experimentally, by striking the reference frame with a pendulum striker of mass 1.7 kg. The contact area was kept 30 x 10 mm to maintain the mass-contact area ratio same as in the frame pounding experiments. The suspended striker was pulled and allowed to impact the frame at 0.075 m/s speed. The test was repeated three times and accelerations of the frame and the striker were measured at a sampling rate of 4 kHz. The impact force time history was calculated from Newton's second law. The time history was applied numerically to the frame and the resultant motion was compared with the actual recorded motion. The average values of coefficient of restitution and contact elements stiffness were calculated and adopted for numerical simulations. The results are discussed in section 4.

4 EXPERIMENTAL RESULTS

The maximum deflections of the reference frame when subjected to various time histories are shown in Figure 5. The scaled NZDS loadings caused the maximum displacement while the scaled JDS loadings have the least frame displacement. The full scale El-Centro time history produced median deflection among the five time-histories in both directions. Ideally, the deflection of the frame without pounding should not be affected by time-histories' direction but it can be seen that there is some slight effect perhaps due to inadvertent lack of symmetry in the model frames.

For the study of pounding effects, a factor μ_{max}/u_{max} is employed where μ_{max} is the maximum deflection of the reference frame when pounding with other frames and u_{max} is the maximum deflection without pounding. Thus μ_{max}/u_{max} is the amplification of maximum deflection due to pounding. Figure 6 shows μ_{max}/u_{max} in the left reference frame. The results show that pounding not only amplified the maximum deflection but also reduced the maximum deflection of the participating frames. In the case of the most demanding time history, NZDS 2, pounding reduced the maximum deflection in all configurations while for NZDS 1, the amplification was seen only for case 2. For JDS and El-Centro time histories, the maximum μ_{max}/u_{max} occurred when the right frame was the most flexible (case 2). It can be seen that, for a given frame pairing, the direction of ground motion can have a significant impact on

μ_{max}/u_{max}. For example, μ_{max}/u_{max} for Case 6 under JDS 1 increased almost 20% higher when the ground motion direction was reversed.

The experimental results agree with the previous numerical studies that μ_{max}/u_{max} of reference frame is highest when the other frame was most flexible (case 2) and least when the other frame was most stiff (case 7). When both frames have the same stiffness, amplification increased with increase in mass (cases 3 to 6). For the similar mass of right frame, the amplification decreased with stiffness (cases 2, 6 and 8). μ_{max}/u_{max} was consistently less than one when T_1/T_2 was greater than 0.8 (cases 1, 4 and 7). The maximum displacement was reduced in all cases under NZDS 1 loading and in all but one case under NZDS 2 loading. Some pounding occurred even when the right frame had the same mass and stiffness as the left reference frame. It could be due to some slight difference in natural frequency even though every effort was made to keep the properties identical. Such pounding caused reduction in maximum displacement under all ground motions.

The results show that the displacement amplification due to pounding is more dependent on the natural periods of the two structures than on the mass. The mass of the right frame was equal in cases 6 and 8 but T_2/T_1 in case 6 was higher and so was μ_{max}/u_{max}. The displacement amplification was nearly equal in cases 5 and 8 which have right frames with different masses but equal natural periods.

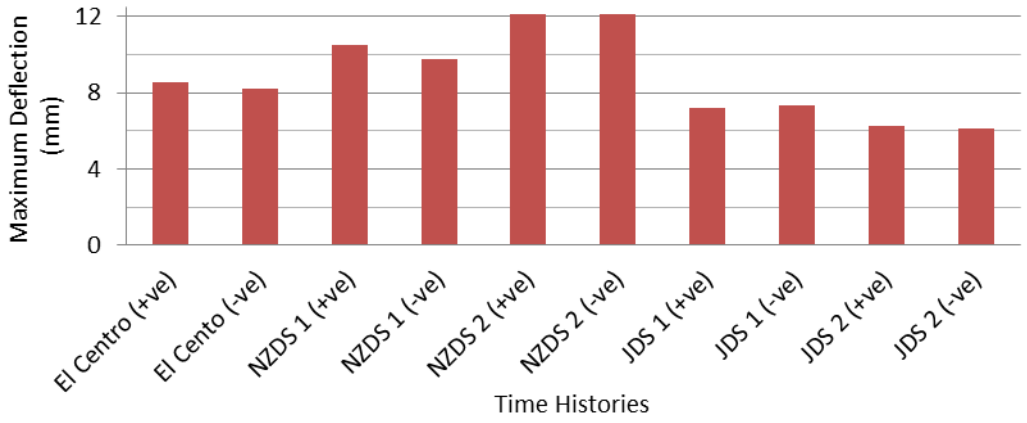

Figure 5. Maximum deflection of the reference frame under time histories considered without pounding effect

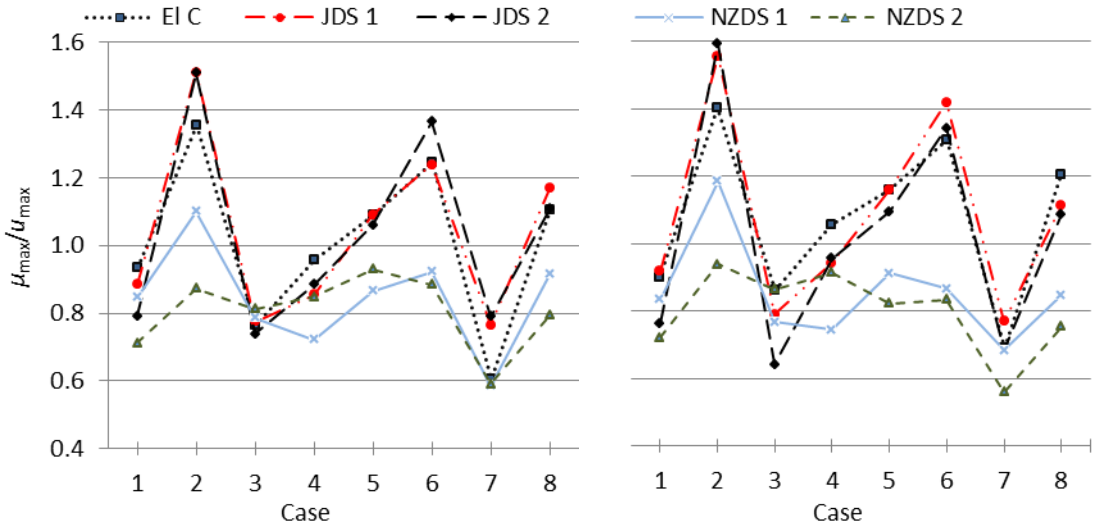

Figure 6. Experimental μ_{max}/u_{max} of the reference frame under five time histories. (a) Positive direction and (b) negative direction

Figures 7 and 8 show the force time history and force-deformation curves from the impact tests conducted to find the coefficient of restitution and impact element stiffness. The coefficient of

restitution was found to be 0.4. The impact element stiffness for each model is calculated by equating total impulse from the simulated and measured force time history. Previous studies have identified these values by equating the maximum force but it was felt that since impact is an impulsive phenomenon, better results may be obtained by equating total impulse. The stiffness calculated for three impact elements are shown in Table 5. The modified linear viscoelastic and modified Hertzdamp models are derivatives of linear viscoelastic and Hertzdamp models respectively and they have been analysed with the same stiffness as their original models.

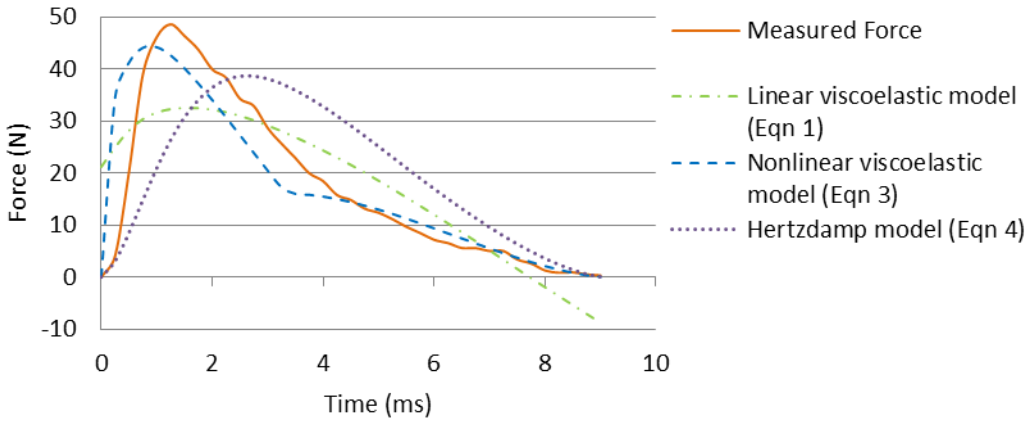

Figure 7. Measured force time history and numerical approximations

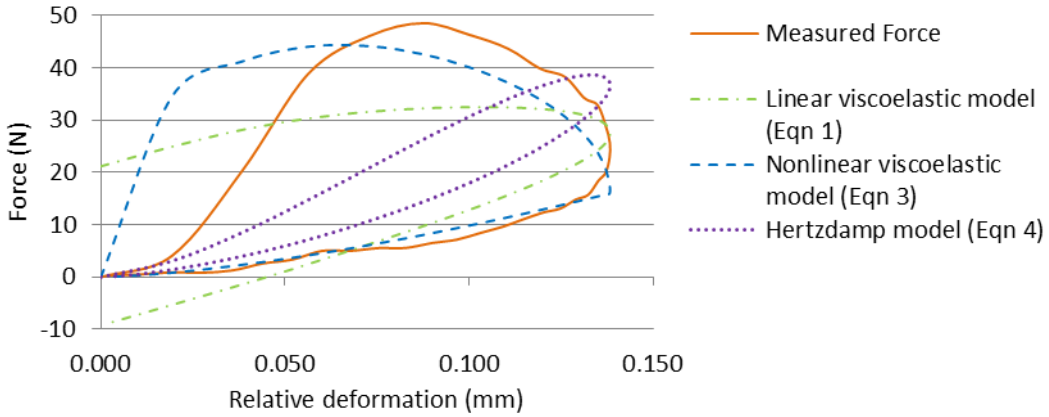

Figure 8. Force-deformation relation for measured force and numerical approximations

Table 5. Coefficient of restitution and impact element stiffness for various models

Impact Element	Stiffness
Linear Viscoelastic model	200,000 N/m
Nonlinear Viscoelastic model	10,000,000 N/m$^{3/2}$
Hertzdamp model	22,500,000 N/m$^{3/2}$

5 NUMERICAL RESULTS AND DISCUSSIONS

The frames employed in the shake table experiments and in the numerical simulations were subjected to the same time histories, and applied from both directions. The simulations were carried out for two coefficients of restitutions values, viz., 0.4 and 0.6. The value, e = 0.4 was found from impact tests, while the value of 0.6 was used as it is the most commonly employed value in numerical studies. Similarly, two contact element stiffness values i.e. 200,000 N/m from Table 5 and 100 times the maximum stiffness of participating structures were employed for the linear viscoelastic and modified

linear viscoelastic elements. The second value was employed to study the effect on displacement amplification due to element stiffness variation. Similarly, for the nonlinear impact elements, three impact stiffness values, viz. value from Table 5, a fifth of this value and five times this value were applied. Thus there were a total of 4 combinations each of e and k for linear models and 6 combinations each for the nonlinear models. The Equation (6) was solved for all these configurations with time-stepping integration at a time step of 0.1 ms.

$$\begin{bmatrix} m_1 & 0 \\ 0 & m_2 \end{bmatrix}\begin{bmatrix} \ddot{x}_1(t) \\ \ddot{x}_2(t) \end{bmatrix} + \begin{bmatrix} C_1 & 0 \\ 0 & C_2 \end{bmatrix}\begin{bmatrix} \dot{x}_1(t) \\ \dot{x}_2(t) \end{bmatrix} + \begin{bmatrix} K_1 & 0 \\ 0 & K_2 \end{bmatrix}\begin{bmatrix} x_1(t) \\ x_2(t) \end{bmatrix} + \begin{bmatrix} x_1(t) \\ x_2(t) \end{bmatrix} + \begin{bmatrix} F(t) \\ -F(t) \end{bmatrix}$$

$$= -\begin{bmatrix} m_1 & 0 \\ 0 & m_2 \end{bmatrix}\begin{bmatrix} \ddot{x}_g(t) \\ \ddot{x}_g(t) \end{bmatrix} \qquad (6)$$

where $\ddot{x}_i(t)$, $\dot{x}_i(t)$, $x_i(t)$, C_i and K_i are the horizontal acceleration, velocity, displacement, damping and stiffness respectively and m_i is the mass of the frame i (i = 1, 2); F(t) is the pounding force given by the particular numerical model while the frames are in contact.

The maximum deflections of the reference frame without pounding were calculated when subjected to various time histories. It was observed that the numerical and experimental deflections in all the cases were very close. There was difference of just 2%-5% between the two values.

Figure 9 shows the comparison of experimental μ_{max}/u_{max} of the reference frame with those calculated by numerical models under positive JDS 2 time history. The results were similar for JDS 1 and El-Centro time histories. The numerical results are plotted only for the best performing contact element stiffness value while the results obtained for both the values of coefficient of restitution are shown for comparison. The contact elements were not very sensitive to change in stiffness of contact but there were some variations. The linear viscoelastic and modified linear viscoelastic elements agreed best with the experimental results when e = 0.4, and k = 100 times maximum of stiffness of the participating structures. The nonlinear contact elements showed the best agreement with the shake table results when the experimentally measured contact element stiffness was used. The amplification was much greater when coefficient of restitution was 0.6 than when it was 0.4. The sensitivity of numerical models to the coefficient of restitution was not consistent. The variation of e affected the amplification much more in some cases than in others.

The results from NZDS ground motions were significantly different from those observed for the JDS and El-Centro loadings. Figure 10 presents the experimental and numerical μ_{max}/u_{max} of the reference frame under positive NZDS 2 loading. The numerical results are for e = 0.4 and k is the same as explained above. The experiment showed a reduction in maximum deflection in all pounding cases but numerical simulations did not reflect this. The trend was similar for all the contact element models for this time history applied through both directions. The displacement amplification was even greater when e = 0.6 for which the results are not shown here. Thus, for the frame configurations considered in this experiment, the commonly adopted value of coefficient of restitution predicted much more severe response than the experimentally determined value, which itself predicted higher displacement response than that from the experiments. The results due to NZDS 1, not presented here, were similar.

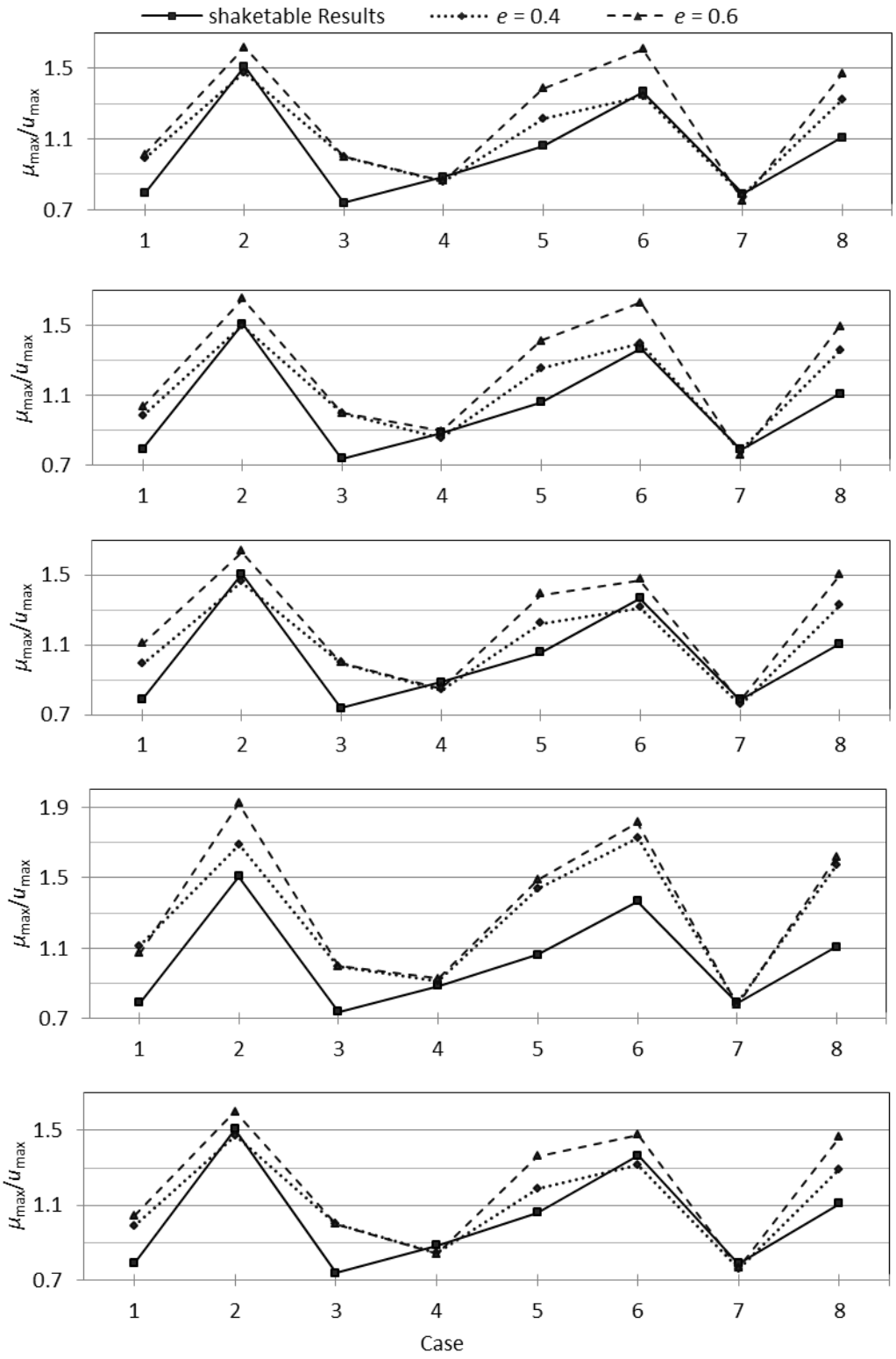

Figure 9. Experimental and numerical μ_{max}/u_{max} of the reference frame under positive JDS 2 ground motion (a) Linear Viscoelastic, (b) Modified Linear Viscoelastic, (c) Nonlinear Viscoelastic, (d) Hertzdamp, and (e) Modified Hertzdamp models

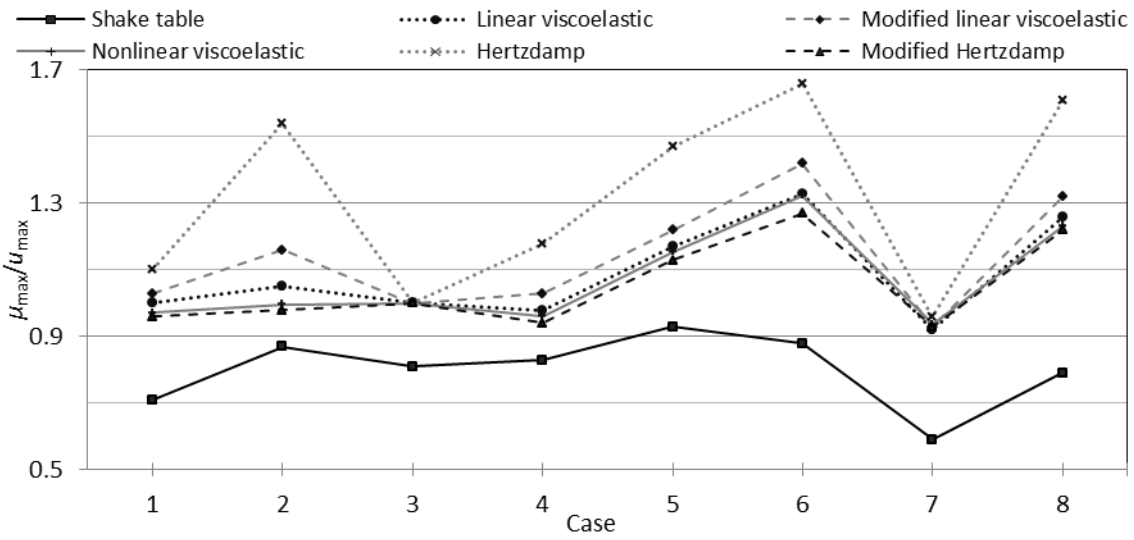

Figure 10. Experimental and numerical μ_{max}/u_{max} of the reference frame under positive NZDS 2 ground motion

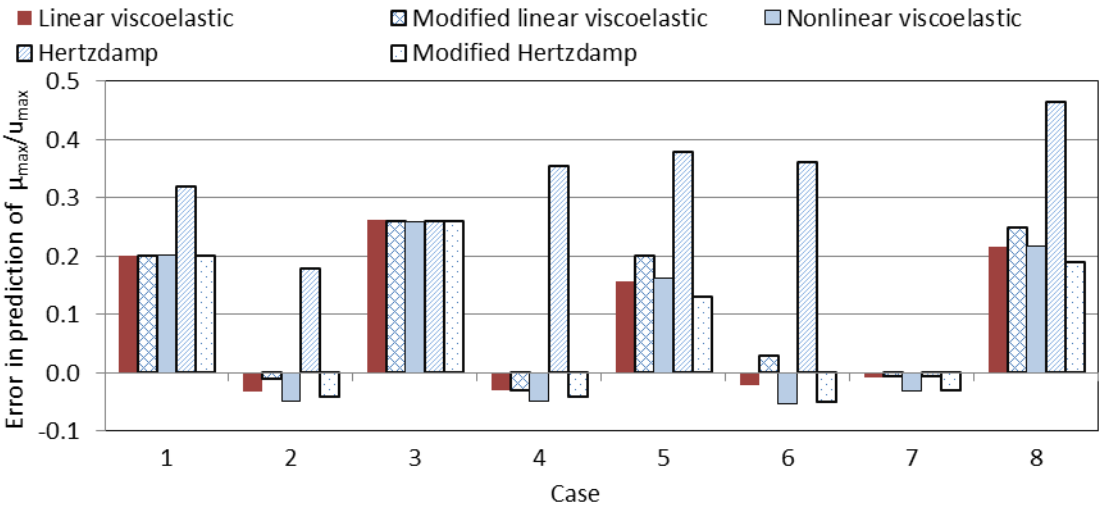

Figure 11. Error in prediction of amplification of maximum displacement under JDS 2 ground excitation

Figure 11 shows the predictive error in μ_{max}/u_{max} from different numerical models subjected to the JDS 2 loading. All the models overestimated the displacement amplification in cases 1, 3, 5 and 8 but the amplification in cases 4, 5, and 7 were predicted quite well by all except Hertzdamp model. The Hertzdamp model seldom underestimated the amplification but tended to overestimate severely in cases 5, 6 and 8. These latter cases are theoretically more hazardous as the reference frame was pounding against more flexible frames. Other four models sometimes underestimated the amplification but the error was under 5%; the modified Hertzdamp model was as accurate as the linear viscoelastic model while the modified linear viscoelastic model generally had slightly higher error.

None of the models predicted consistently better than all others in all configurations; hence a simple criterion was applied to choose the best model. Figure 12 shows the plot of square root of sum of square (SRSS) of errors across all cases for all time histories. Four of the models perform very similarly but Hertzdamp model has almost twice the error magnitude.

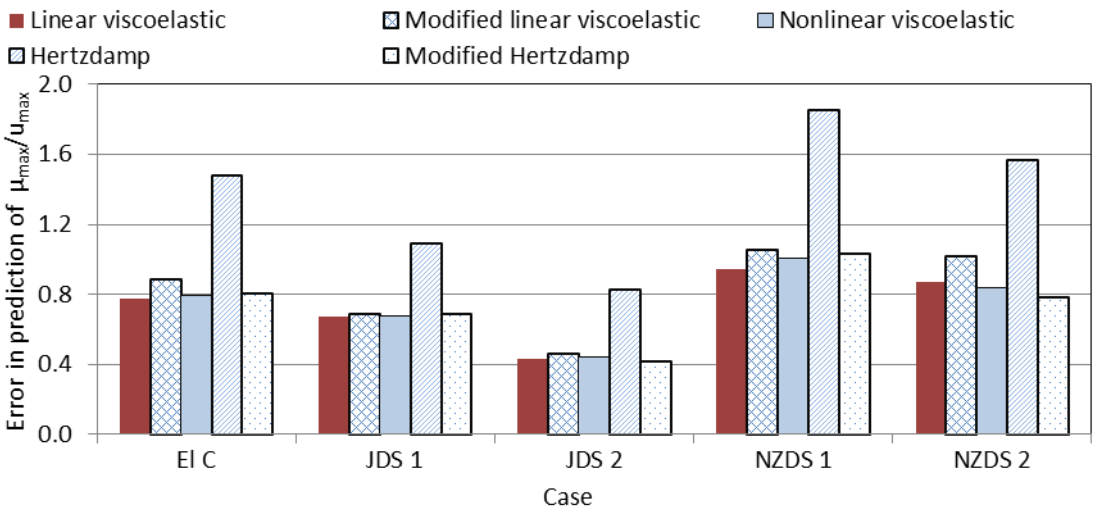

Figure 12. SRSS of errors in μ_{max}/u_{max} from various models

From the discussion in Section 2, it can be seen that the newer models are much more complicated than the linear viscoelastic element. But the results show that the added complexity in newer models do not increase their accuracy. Thus linear viscoelastic contact element is recommended to be used in future numerical modelling of floor to floor pounding of two structures. The model underestimates the severity of response amplification in some cases but the safety factors available in design of structures should be able to withstand a variation of 10%. Additionally, this model can already be found implemented as a linear viscoelastic link in most of the commercial design software.

6 CONCLUSIONS

A shake table investigation on pounding between a pair of steel portal frames was conducted to evaluate the performance of five numerical pounding force models. The frames were constructed such that their masses and stiffness could be varied. A frame with mass 8.6 kg and stiffness 8.9 kN/m was designated the reference frame, and the mass and stiffness of second frame was changed to produce different natural period ratio. A total of eight frame pairs were tested. Five ground motions were applied to each pair of frames and the displacement response of the frames was recorded. Each test was repeated with the same ground motions applied in reverse direction. The same ground motions, from both directions, were applied to each frame in isolation, to identify their displacement response without pounding. For each frame pair amplification of maximum displacement was calculated as the ratio of maximum displacement of the reference frame to the maximum displacement without pounding.

Numerical simulations were conducted for pounding of the frame pairs under each of the ground motions employed in the experiment. The amplification of maximum displacement was calculated for the five force models. From the comparison of predicted and actual amplification, following conclusions can be drawn:

- The best agreement between experimental and numerical values of deflection amplification is obtained from the linear viscoelastic element. All other models, though some of them are much more complex in numerical implementation, showed similar behavior. The Hertzdamp model is highly inaccurate in these simulations which was as expected, as the model was originally formulated for highly elastic impacts.
- None of the numerical models are sensitive to the change in contact element stiffness when predicting displacement amplifications. The models are sensitive to the change in coefficient of restitution, but no pattern could be identified. The numerical models were highly conservative for coefficient of restitution 0.6 which is the most commonly adopted in past studies. Much better agreement with test results was observed when a value of 0.4 was adopted.

- The shake table results show agreement with the numerical models that the amplification of maximum displacement is more when the test frame collides with a more flexible adjacent frame and displacement is reduced when it collides with more rigid frames. But the numerical models mostly predict a higher amplification than observed in the experiments. Thus the current numerical models seem to overestimate the severity of displacement amplification due to seismic pounding.
- The displacement amplification due to pounding is higher if the difference in natural periods is higher. The mass difference between the two frames did not show as much effect as the frequency difference.
- All numerical models were unable to simulate the reduced displacement for some of the time histories. A pattern was observed where the ground motions that produced higher displacement without pounding experienced less amplification due to pounding. Further experiments with many more ground motions will be required to ascertain if this is due to frequency content of the ground motions or a general behavior.

The study does not measure or compare the pounding force as most of the force measuring devices tend to alter the structural properties or the contact interface. Similarly, no microscopic study of the contact surface was conducted after the impact to quantify the surface deformation after pounding. The tests conducted were very small scale compared to the actual structures that experience pounding, so some large scale tests will be required to assess if the same trend is applicable to building pounding during earthquakes.

ACKNOWLEDGEMENTS

The first author is deeply indebted to The University of Auckland for his International Doctoral Scholarship.

REFERENCES

Anagnostopoulos, S.A. 1988. Pounding of buildings in series during earthquakes. *Eathquake Engineering and Structural Dynamics*, Vol 16(3): 443-456.

Anagnostopoulos, S.A. & Karamaneas C.E. 2008. Use of collision shear walls to minimize seismic separation and to protect adjacent buildings from collapse due to earthquake induced pounding. *Earthquake Engineering & Structural Dynamics* Vol 37(12):1371-1388.

Bothara, J.K., Jury, R.D., Wheeler, K. & Stevens, C. 2008. Seismic Assessment Of Buildings In Wellington: Experiences And Challenges. *Proceedings of The Fourteenth World Conference on Earthquake Engineering*. Beijing, China.

Cole, G.L., Dhakal, R.P. & Turner F.M. 2012. Building pounding damage observed in the 2011 Christchurch earthquake. *Earthquake Engineering & Structural Dynamics,* Vol 41(5): 893-913.

Chau, K.T., Wei, X.X. Guo, X. & Shen, C.Y. 2003. Experimental and theoretical simulations of seismic poundings between two adjacent structures. *Earthquake Engineering & Structural Dynamics,* Vol 32(4): 537-554.

Chouw, N. (2002). Influence of soil-structure interaction on pounding response of adjacent buildings due to near-source earthquakes, *JSCE Journal of Applied Mechanics*, Vol. 5, 543-553

Chouw, N. & Hao, H. 2012. Pounding damage to structures in the 2011 Christchurch earthquake, *International Journal of Protective Structures* **3**(2): 123-139, 2012

Chouw, N. & Hao, H. 2008. Significance of SSI and nonuniform near-fault ground motions in bridge response I: Effect on response with conventional expansion joint. *Engineering Structures,* Vol 30(1): 141-153.

Filiatrault, A., Wagner, P. & Cherry, S. Analytical prediction of experimental building pounding. *Earthquake Engineering & Structural Dynamics,* Vol 24(8):1131-54.

Goldsmith W. 2001. *Impact: the theory and physical behaviour of colliding solids*, New York: Dover Publications.

Jankowski R. 2005. Non linear viscoelastic modelling of earthquake induced structural pounding. *Earthquake*

Engineering & Structural Dynamics, Vol 34(6): 595-611.

Jankowski, R. Analytical expression between the impact damping ratio and the coefficient of restitution in the non linear viscoelastic model of structural pounding. *Earthquake Engineering & Structural Dynamics*, Vol 35(4): 517-24.

Jeng, V. & Tzeng, W.L. 2000. Assessment of seismic pounding hazard for Taipei City. *Engineering Structures*, Vol 22(5): 459-471.

Kasai, K. & Maison, B.F. 1997. Building pounding damage during the 1989 Loma Prieta earthquake. *Engineering Structures*, Vol 19(3): 195-207.

Mahmoud, S. 2008. Modified linear viscoelastic model for elimination of the tension force in the linear viscoelastic. *Proceedings of Fourteenth World Conference on Earthquake Engineering*. Beijing, China.

Mahmoud, S. & Jankowski, R. 2011. Modified linear viscoelastic model of earthquake-induced structural pounding. *IJST, Transactions of Civil and Environmental Engineering*, Vol 35(C1): 55-62.

Muthukumar, S. and DesRoches, R. 2006. A Hertz contact model with non linear damping for pounding simulation. *Earthquake Engineering & Structural Dynamics*, Vol 35(7): 811-828.

Papadrakakis, M. and Mouzakis, H.P. 1995. Earthquake simulator testing of pounding between adjacent buildings. *Earthquake Engineering & Structural Dynamics*, Vol 24(6): 811-834.

Papadrakakis, M., Mouzakis, H., Plevris, N. & Bitzarakis, S. 1991. A Lagrange multiplier solution method for pounding of buildings during earthquakes. *Earthquake Engineering & Structural Dynamics*,Vol 20(11): 981-998.

Rezavandi, A. & Moghadam, A.S. 2007. Experimental and numerical study on pounding effects and mitigation techniques for adjacent structures. *Advances in Structural Engineering*, Vol 10(2): 121-34.

Rosenblueth, E. & Meli, R. 1986. The 1985 earthquake: causes and effects in Mexico City. *Concrete International*, Vol 8(5): 23-34.

Valles-Mattox, R. & Reinhorn, A. 1996. Evaluation, prevention and mitigation of pounding effects in building structures. *Proceedings of Eleventh World Conference on Earthquake Engineering*. Acapulco, Mexico.

van Mier, J.G.M., Pruijssers, A.F., Reinhardt, H.W., & Monnier, T. 1991. Load Time Response of Colliding Concrete Bodies. *Journal of Structural Engineering*, Vol 117(2): 354-374.

Ye, K., Li, L., & Zhu, H. 2009. A note on the Hertz contact model with nonlinear damping for pounding simulation. *Earthquake Engineering & Structural Dynamic*, Vol 38(9): 1135-1142.